Perovskite solar cells with CuI inorganic hole conductor

Kenta Takahashi[1] and Yoshikazu Suzuki[1, 2*]

[1]*Graduate School of Pure and Applied Sciences, University of Tsukuba, Ibaraki 305-8573, Japan*

[2]*Faculty of Pure and Applied Sciences, University of Tsukuba, Ibaraki 305-8573, Japan*

[*]E-mail: suzuki@ims.tsukuba.ac.jp

Abstract

An organic material, 2,2',7,7'-tetrakis(N,N-di-p-methoxyphenylamine)9,9'-spirobifluorene (spiro-OMeTAD), is generally used as a hole conductor of perovskite solar cells (PSCs), but spiro-OMeTAD is much more expensive than other materials used in PSCs. In this study, we have prepared PSCs with a cost-effective CuI hole transport layer by spin coating. The merit of using spin coating for CuI is good compatibility with other steps, such as spin coating of a TiO$_2$ electron transport layer and a perovskite active layer. The CuI-based PSC recorded power conversion efficiencies of $\eta =2.22\%$ (max) on the day of production and $\eta =6.52\%$ (max) after the 20 days of production. Moreover, the CuI-based PSC had a smaller hysteresis than the spiro-based PSC, suggesting that CuI is a highly promising alternative hole conductor for PSCs.

1. Introduction

Perovskite solar cells (PSCs) were first reported by Kojima et al. with a power conversion efficiency (PCE) of 3.81% in 2009.[1)] Recently, the PCE of PSCs has been much improved to 22.1%,[2)] and thus PSCs are focused all over the world. Figure 1(a) shows a conventional structure of PSCs. PSCs are commonly composed of a transparent conductive oxide glass, an electron transport layer (ETL) made from compact and mesoporous oxide films (TiO$_2$ or ZnO), a perovskite active layer (ABX$_3$, A=CH$_3$NH$_3$, B=Pb or Sn, X=I, Cl, or Br), a hole transport layer (HTL), and a metallic electrode (Au, Ag, or Al). Among these layers, we focused on the HTL. In general, an organic material, 2,2',7,7'-tetrakis(N,N-di-p-methoxyphenylamine)9,9'-spirobifluorene (spiro-OMeTAD), is used as a hole conductor,

and the solar cells using spiro-OMeTAD demonstrate high photovoltaic performances.[3-5] However, spiro-OMeTAD is very expensive, i.e., over 10 times more expensive (per mass) than the other materials used in PSCs.

As an alternative hole conductor in PSCs, several organic and inorganic materials, such as poly(triarylamine) (PTAA),[6] poly(3-hexylthiophene) (P3HT),[7] poly[(9,9-dioctylfluorenyl-2,7-diyl)-co-(4,4'-(N-(4-*sec*-butylphenyl)diphenylamine)] (TFB),[8] CuSCN,[9-12] NiO,[13-15] CuO-Cu$_2$O[16-18] and CuI,[19-21] have been tested. Among these candidates, CuI is focused in this study by following features:

(1) low cost (~1/500 of spiro-OMeTAD),

(2) conduction band position similar to the HOMO level of spiro-OMeTAD [22, 23] (Fig. 1(b)),

(3) much higher hole mobility (CuI: 0.5-2 cm^2 V^{-1} s^{-1},[24] spiro-OMeTAD: ~2×10^{-4} cm^2 V^{-1} s^{-1} [25,26]),

(4) thin film deposition at low temperatures (near room temperature),[24, 27] and

(5) p-type semiconductor (zinc blend structure) with a wide bandgap of ~3.1 eV below 350 °C.[28]

Christians et al. [19] reported the preparation of a CuI HTL by automated drop casting (modified doctor blade method), which resulted in a power conversion efficiency (PCE) of 6.0% in 2014. Sepalage et al.[20] also reported the preparation of the CuI HTL by a manual doctor blade method with a PCE of 7.5% in 2015. Huangfu et al.[21] prepared a CuI thick film HTL by spraying with a PCE of 5.8% in 2015. Recently, Hossain et al.[29] have evaluated the optimum thicknesses of several HTLs by a computation method, and pointed out that ~200 nm is the optimum thickness of the CuI HTL.

To control the film thickness of CuI, spin coating will be easy and effective. Thus, in this study, we have prepared the CuI HTL by spin coating. Another merit of using spin coating for CuI is good compatibility with other steps, such as spin coating of a TiO$_2$ ETL and a perovskite active layer. Furthermore, the aging effect (up to 40 days) was evaluated.

2. Experimental methods

2.1 Cell preparation

Etched ITO glass (Geomatic, type 0052, 10 Ω/sq.) was rinsed with distilled water and then with ethanol for 5 min. **A** TiO$_2$ compact layer was prepared on the ITO glass by spin coating 0.15 M titanium diisopropoxide bis(acetylacetonate) (75% in isopropanol, Sigma-Aldrich) solution in 1-butanol at 2000 rpm for 20 s and annealed at 125°C for 5 min. Then, this process

was repeated twice with 0.3 M diisopropoxide bis(acetylacetonate) (75% in isopropanol) solution. The substrate was annealed at 500°C for 15 min in air.

A commercial TiO_2 paste (Dyesol, 18NR-T) was diluted 5 times with ethanol. A TiO_2 mesoporous layer was prepared on the TiO_2 compact layer by spin coating the diluted TiO_2 paste at 4000 rpm for 25 s and annealed at 500°C for 30 min in air. From our preliminary test, 1-time TiO_2 mesoporous layer coating was suitable for spiro-based PSCs, and 3-time TiO_2 mesoporous layer coatings were suitable for CuI-based PSCs. For each of the 3-time TiO_2 mesoporous layer coating, the annealing time was 10 min; thus, the total annealing time was 30 min. Then, each substrate was immersed in 40 mM $TiCl_4$ solution in distilled water at 70°C for 30 min, rinsed with ethanol, and annealed at 500°C for 45 min in air.

A perovskite ($CH_3NH_3PbI_3$) active layer was prepared by a two-step method in air under 35% humidity. PbI_2 (>98.0%, Tokyo Chemical Industry) was dissolved in N,N-dimethylformamide (DMF; 99.5%, Nacalai Tesque). PbI_2 solution (1 M) was spin- coated on the TiO_2 mesoporous layer at 3000 rpm for 20 s and annealed at 80°C for 10 min on a hot plate in air. Then, the substrate was immersed in 10 mg/mL CH_3NH_3I solution (98%, Wako Pure Chemical Industry) in 2-propanol (99.5%, Nacalai Tesque) for 40 s, rinsed in 2-propanol and annealed at 80°C for 10 min in air.

As for the HTL, both spiro-OMeTAD (as a control) and CuI were prepared. A spiro-OMeTAD HTL was prepared by spin coating (at 4000 rpm for 35 s) spiro-OMeTAD solution (~57 mM) consisting of 73 mg of spiro-OMeTAD (99%, Sigma-Aldrich), 28.8 µL of 4-*tert*-butylpyridine (TBP; 96.0%, Sigma-Aldrich), and 17 µL of 520 mg/mL lithium bis(trifluoromethylsulfonyl)imide salt solution (98.0%, Tokyo Chemical Industry) in acetonitrile (99.5%, Wako Pure Chemical Industry) in 1 mL of chlorobenzene (99%, Nakalai Tesque). The CuI HTL was prepared by spin coating (at 2000 rpm for 35 s) CuI solution (0.1 M); CuI powder ($\geqq$99.5%, Sigma-Aldrich) was dissolved in a chlorobenzene/acetonitrile/4-*tert*-butylpyridine solution at 40:20:1 (in volume ratio). Finally, a gold electrode was deposited by thermal evaporation on top of each device under a pressure of ~1.0×10^{-5} Torr.

2.2 Cell evaluation

The starting CuI powder, CuI film directly deposited on ITO (by dropping), and prepared solar cells were analyzed by X-ray diffraction (XRD; Rigaku Multiflex, CuK_α, 40 kV and 40 mA). Current density-voltage (*J-V*) characteristics were measured with a solar simulator (San-ei Electric XES-40S1), calibrated to AM 1.5, 100 mW/cm^2 with a standard silicon

photodiode (Bunkokeiki BS-520BK). The active area was 0.087 cm^2 with a black mask. The voltage step and delay time were 20 mV and 50 ms, respectively. Three spiro-based and ten CuI-based PSCs were prepared. Photovoltaic performance was measured at 2 points in each cell, and therefore, 6 and 20 data sets were obtained for spiro-based and CuI- based PSCs, respectively. In this paper, the average and the maximum performances of these cells were discussed. The CuI powder and the surfaces of the perovskite active layer and CuI HTL were observed by scanning electron microscopy (SEM; Hitachi High-Technologies SU-70 and JEOL JSM-5600LV).

3. Results and discussion

3.1 Phase analysis

Figure 2(a) shows XRD patterns of CuI powder and a CuI 'thick' film deposited by dropping CuI solution on the ITO glass. The XRD pattern of the CuI thick film contained a 111 strong reflection as reported by Cai et al.[30] This result confirms that a CuI 'thin' film can be formed by spreading droplets via spin coating. Figure 2(b) shows XRD patterns of the spiro-based and CuI-based PSCs. CH$_3$NH$_3$PbI$_3$ peaks were clearly observed for both cells, with some unreacted (or decomposed) PbI$_2$ peaks, as frequently reported for the 2-step method in the literature. Throughout the XRD study, CuI spin coating did not significantly damage the perovskite layer.

3.2 *J-V* characteristics

Figure 3 shows *J-V* curves of the prepared cells: (a) spiro-based PSC (0 day), (b) CuI-based PSC (0 day), (c) spiro-based PSC (after 21 days) and (d) CuI-based PSC (after 20 days). The *J-V* curves showing the highest performance are plotted in each figure. Inset values are for the best performance: (a), (c), and (d) are for the back scan, and (b) is for the forward scan. Figures 3(a) and 3(b) show the values measured on the day of cell production. Table I summarizes the cell performance. By comparing Figs. 3(a) and 3(b) (i.e., 0 day), the CuI-based PSCs were found to initially show a much lower efficiency than the spiro-based PSCs (ave. 9.16% and max. 10.5% for the spiro-based PSCs, and ave. 1.00% and max. 2.22% for the CuI-based PSCs.)

To determine whether the CuI-based PSCs have the aging effect, the photovoltaic performance was intermittently measured after cell production. All cells were stored in air under a dark condition, and humidity and temperature were kept at ~40% and ~30°C,

respectively. Figures 3(c) and 3(d) show *J-V* curves of the spiro-based PSC after 21 days of production and those of the CuI-based PSC after 20 days of production, respectively. The highest efficiency of the spiro-based PSC was 9.02%, whereas that of the CuI-based PSC was 6.52%, which was ~72% that of the spiro-based PSC, indicating that the CuI-based PSC had a positive aging effect. The *J-V* hystereses of the PSCs are also plotted in Fig. 3, where dotted and solid lines indicate forward and back scans, respectively. The *J-V* hysteresis of the CuI-based PSC was much smaller than that of the spiro-based PSCs. Sepalage et al. [20] have recently explained that the smaller hysteresis of the CuI-based PSC is attributed to the smaller local electric field generated in the perovskite/CuI system. With aging for 20 days, the hysteresis of the CuI-based PSC became slightly larger, but much smaller than that of the spiro-based PSC [Figs. 3(c)-(d)]. This smaller hysteresis is a merit to use the CuI HTL.

Figure 4 shows the aging effects (up to 40 days) of photovoltaic parameters (average values) of spiro- and CuI-based PSCs. For spiro-based PSCs, all parameters remained almost constant or decreased with aging. This is considered a crucial disadvantage of PSCs. On the other hand, for CuI-based PSCs, all parameters remained almost constant or slightly increased with aging. After ~40 day aging, the PCEs of spiro- and CuI-based PSCs were not quite different to each other. This is probably because the contact between the CuI HTL and the perovskite laye,r and that between the CuI HTL and the Au electrode improved with aging, resulting in an enhanced hole transportation, which is suggested by the *FF* improvement curve in Fig. 4(c).

To consider the performance results of CuI-based PSCs in Figs. 3 and 4, SEM observation was conducted. Figure 5 shows SEM images of (a) the starting CuI powder, (b) the surface of $CH_3NH_3PbI_3$ layer, and (c) the surface of CuI layer on $CH_3NH_3PbI_3$. The particle size of the starting CuI powder was ~10-50 µm [Fig. 5(a)], and the CuI powder completely dissolved in the solvent (i.e., chlorobenzene, acetonitrile, and TBP). The particle size of the $CH_3NH_3PbI_3$ active layer (without a CuI HTL/Au electrode) was ~100-500 nm [Fig. 5(b)]. As shown in Fig. 5(c), the spin-coated CuI thin film covered the $CH_3NH_3PbI_3$ active layer; however, some uncovered areas also existed. Actually, the CuI HTL in this study was difficult to visualize from cross-sectional SEM images (Fig. 6). Therefore, some $CH_3NH_3PbI_3$ crystals may directly be in contact with the Au electrode, where the recombination between electrons (in the active layer) and holes (in the active layer and Au electrode) may occur.

Finally, different coating methods for CuI-based PSCs are listed in Table II. If we can optimize the coating conditions to suppress the direct contact, further improvement in PCE

for CuI-based PSCs is expected.

4. Conclusions

In this study, we have prepared PSCs with a CuI HTL as a cost-effective hole conductor. The CuI-based PSC recorded η =2.22% (max.) on the day of production and η =6.52% (max.) after 20 days of production, whereas the spiro-based PSC (reference) recorded η =10.5% (max.) on the day of production and η =9.02% (max.) after 21 days of production. These results indicate that the CuI-based PSC had a positive aging effect. Moreover, the CuI-based PSC had a smaller hysteresis than the spiro-based PSC. Throughout this study, CuI is highly promising as a hole conductor for PSCs. We expect that the CuI-based PSC will be further improved by the optimization of coating processes.

References
1) A. Kojima, K. Teshima, Y. Shirai, and T. Miyasaka: J. Am. Chem. Soc. **131**, 6050 (2009).
2) https://www.nrel.gov/pv/assets/images/efficiency-chart.png
3) J. Burschka, N. Pellet, S.-J. Moon, R. Humphry-Baker, P. Gao, M. K. Nazeeruddin, and M. Grätzel: Nature **499**, 316 (2013).
4) T. Leijtens, B. Lauber, G. E. Eperon, S. D. Stranks, and H. J. Snaith: J. Phys. Chem. Lett. **5**, 1096 (2014).
5) W. Ke, G. Fang, J. Wang, P. Qin, H. Tao, H. Lei, Q. Liu, X. Dai, and X. Zhao: ACS Appl. Mater. Interfaces **6**, 15959 (2014).
6) S. Ryu, J. Seo, S. S. Shin, Y. C. Kim, N. J. Jeon, J. H. Noh, and S. I. Seok: J. Mater. Chem. A **3**, 3271 (2015).
7) A. Abrusci, S. D. Stranks, P. Docampo, H.-L. Yip, A. K.-Y. Jen, and H. J. Snaith: Nano Lett. **13**, 3124 (2013).
8) Z. Zhu, Y. Bai, H. K. H. Lee, C. Mu, T. Zhang, L. Zhang, J. Wang, H. Yan, S. K. So,

and S. Yang: Adv. Funct. Mater. **24**, 7357 (2014).

9) P. Qin, S. Tanaka, S. Ito, N. Tetreault, K. Manabe, H. Nishino, M. K. Nazeeruddin, and M. Grätzel: Nat. Commun. **5**, 1 (2014).

10) S. Ye, W. Sun, Y. Li, W. Yan, H. Peng, Z. Bian, Z. Liu, and C. Huang: Nano Lett. **15**, 3723 (2015).

11) S. Chavhan, O. Miguel, H.-J. Grande, V. Gonzalez-Pedro, R. S. Sánchez, E. M. Barea, I. Mora-Seró, and R. Tena-Zaera: J. Mater. Chem. A **2**, 12754 (2014).

12) M. Jung, Y. C. Kim, N. J. Jeon, W. S. Yang, J. Seo, J. H. Noh, and S. I. Seok: ChemSusChem **9**, 2592 (2016).

13) Z. Zhu, Y. Bai, T. Zhang, Z. Liu, X. Long, Z. Wei, Z. Wang, L. Zhang, J. Wang, F. Yan, and S. Yang: Angew. Chem., Int. Ed. **53**, 12571 (2014).

14) Z. Liu, M. Zhang, X. Xu, L. Bu, W. Zhang, W. Li, Z. Zhao, M. Wang, Y.-B. Cheng, and H. He: Dalton Trans. **44**, 3967 (2015).

15) S. Seo, I. J. Park, M. Kim, S. Lee, C. Bae, H. S. Jung, N. G. Park, J. Y. Kim, and H. Shin: Nanoscale **8**, 11403 (2016).

16) C. Zuo and L. Ding: Small **11**, 5528 (2015).

17) W. Yu, F. Li, H. Wang, E. Alarousu, Y. Chen, B. Lin, L. Wang, M. N. Hedhili, Y. Li, K. Wu, X. Wang, O. F. Mohammed, and T. Wu: Nanoscale **8**, 6173 (2016).

18) B. A. Nejand, V. Ahmadi, S. Gharibzadeh, and H. R. Shahverdi: ChemSusChem **9**, 302 (2016).

19) J. A. Christians, R. C. M. Fung, and P. V. Kamat: J. Am. Chem. Soc. **136**, 758 (2014).

20) G. A. Sepalage, S. Meyer, A. Pascoe, A. D. Scully, F. Huang, U. Bach, Y.-B. Cheng, and L. Spiccia: Adv. Funct. Mater. **25**, 5650 (2015).

21) M. Huangfu, Y. Shen, G. Zhu, K. Xu, M. Cao, F. Gu, and L. Wang: App. Surf. Sci. **357**, 2234 (2015).

22) W. Sun, H. Peng, Y. Li, W. Yan, Z. Liu, Z. Bian, and C. Huang: J. Phys. Chem. C **118**,

16806 (2014).

23) F. Hao, C. C. Stoumpos, R. P. H. Chang, and M. G. Kanatzidis: J. Am. Chem. Soc. **136**, 8094 (2014).

24) S. Inudo, M. Miyake, and T. Hirato: Phys. Status Solidi A **210**, 2395 (2013).

25) D. Poplavskyy and J. Nelson: J. Appl. Phys. **93**, 341 (2003).

26) L. Schmidt-Mende and M. Grätzel: Thin Solid Films **500**, 296 (2006).

27) K. Tennakone, G. R. R. A. Kumara, I. R. M. Kottegoda, V. P. S. Perera, G. M. L. P. Aponsu, and K. G. U. Wijayantha: Sol. Energy Mater. Sol. Cells **55**, 283 (1998).

28) M. N. Amalina, N. A. Rasheid, and M. Rusop: J. Nanomater. **2012**, 637637 (2012).

29) M. I. Hossain, F. H. Alharbi, and N. Tabet: Sol. Energy **120**, 370 (2015).

30) C. F. Cai, X.-Q. Meng, F.-M. Wu, and Y. Z. Fang: Chin. J. Lumin. **34**, 721 (2013).

Figure Captions

Fig. 1. (Color online) (a) Conventional structure and (b) energy diagram of PSCs.

Fig. 2. (Color online) XRD patterns of (a) CuI powder/ thick film on the glass and (b) PSCs (HTM: spiro-OMeTAD or CuI).

Fig. 3. J-V curves of the prepared cells: (a) spiro based PSC (0 day), (b) CuI based PSC (0 day), (c) spiro based PSC (21 days) and (d) CuI based PSC (20 days). The J-V curves showing the highest performance are plotted in each figure. Inset values are for the highest performance: (a), (c), and (d) are for the back scan, and (b) is for the forward scan.

Fig. 4. (Color online) Aging effects of the photovoltaic parameters. (J_{sc}, V_{oc}, η, and FF).

Fig. 5. SEM images of (a) starting CuI powder, (b) surface of $CH_3NH_3PbI_3$ layer, and (c) surface of CuI layer on $CH_3NH_3PbI_3$

Fig. 6. Cross-sectional SEM images: (a) spiro-based PSC (TiO$_2$~200 nm thickness / $CH_3NH_3PbI_3$~450 nm / spiro-OMeTAD~150 nm) and
(b) CuI-based PSC (TiO$_2$~500 nm thickness / $CH_3NH_3PbI_3$+CuI~500 nm).

Table I. Characteristics of prepared PSCs (measured on the same day of cell production).

HTM		J_{SC} (mA/cm^2)	V_{OC} (V)	PCE (%)	FF
spiro-OMeTAD	Ave	16.9 ±1.1	0.83 ±0.02	9.16 ±1.05	0.66 ±0.03
	Max	18.4	0.85	10.5	0.68
CuI (0.1 M)	Ave	11.0 ±2.15	0.36 ±0.04	1.00 ±0.46	0.34 ±0.04
	Max	14.7	0.42	2.22	0.40

Table II. CuI based PSCs prepared by different coating methods.

CuI coating methods	CuI thickness	Maximum PCE (%)	Ref.
Automated dropcasting	1.5-2.0 μm	6.0	Christians et al.[19]
Manual doctor blade	~400 nm	7.5	Sepalage et al.[20]
Spray coating	17.5 ± 1.5 μm	5.8	Huangfu et al.[21]
Spin coating + aging	< 100 nm [a]	6.5	This study

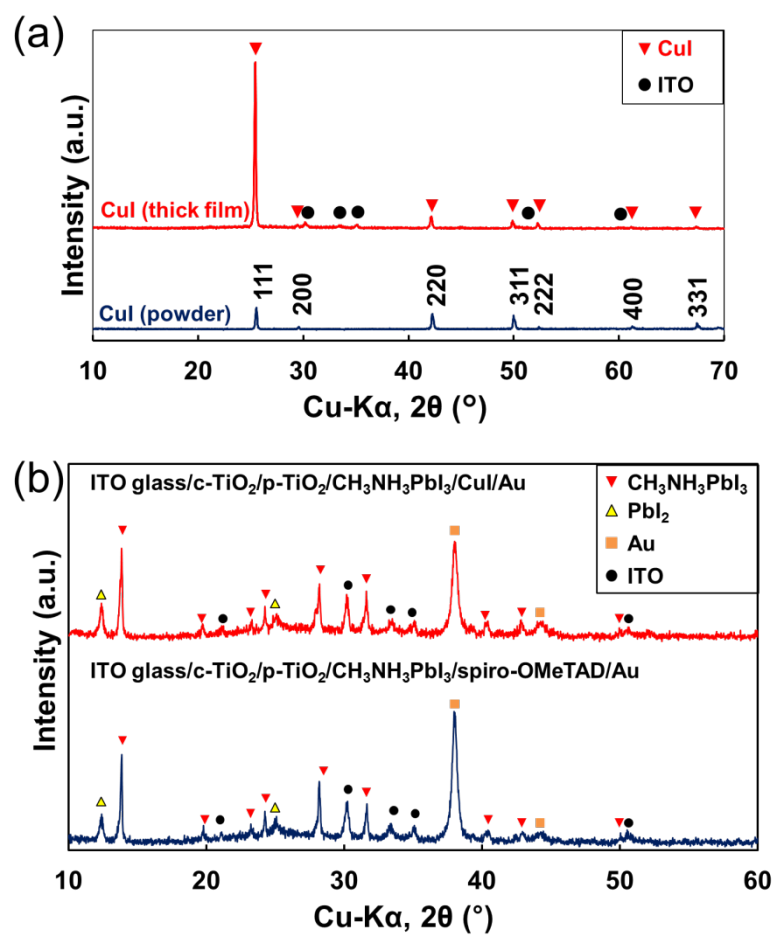[a] Mostly embedded between perovskite crystals
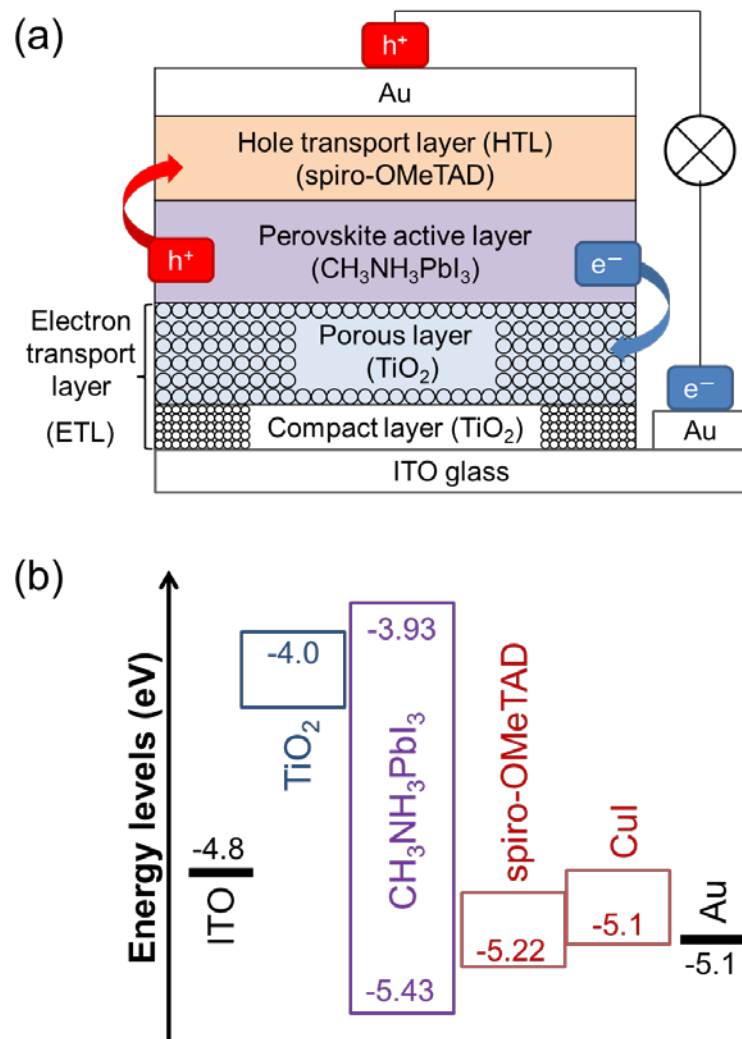
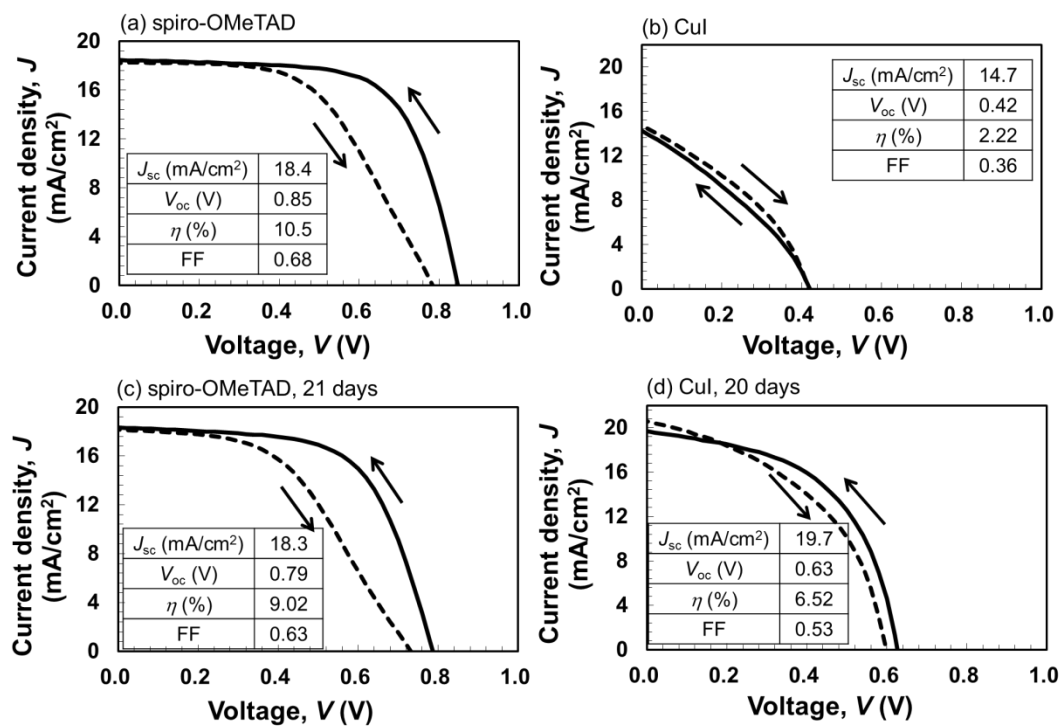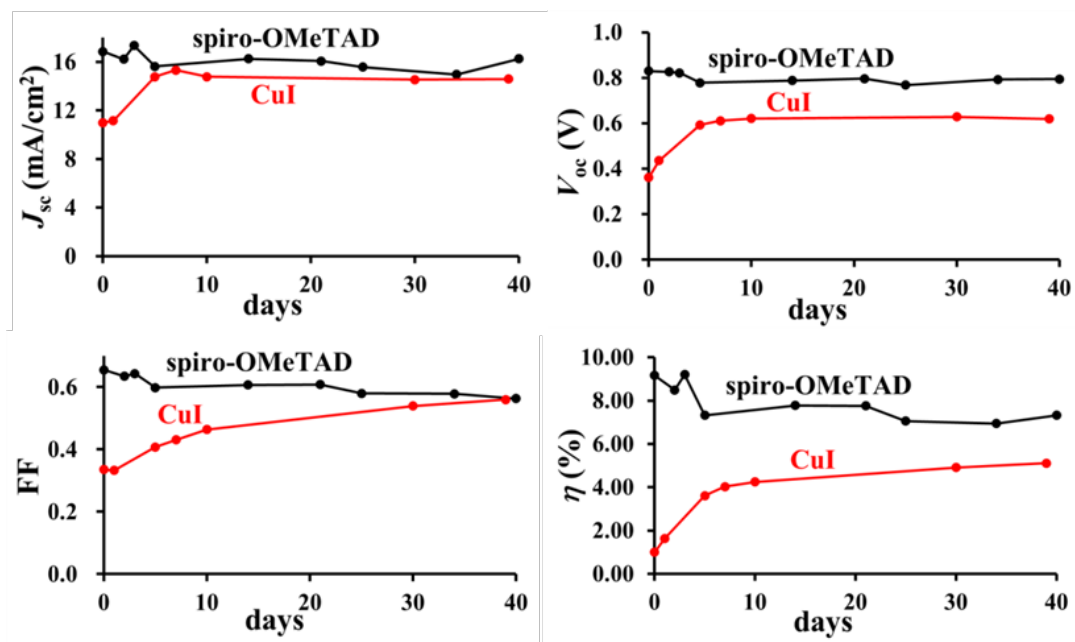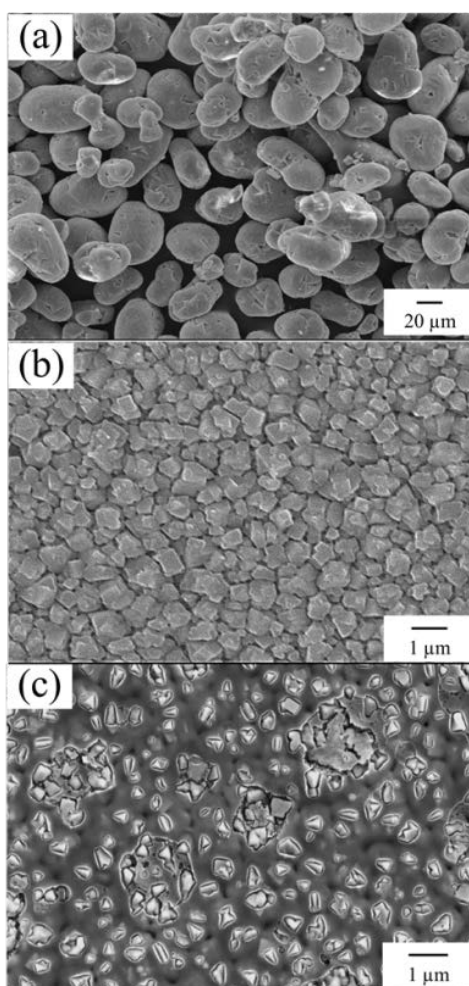Fig. 1. (Color online)

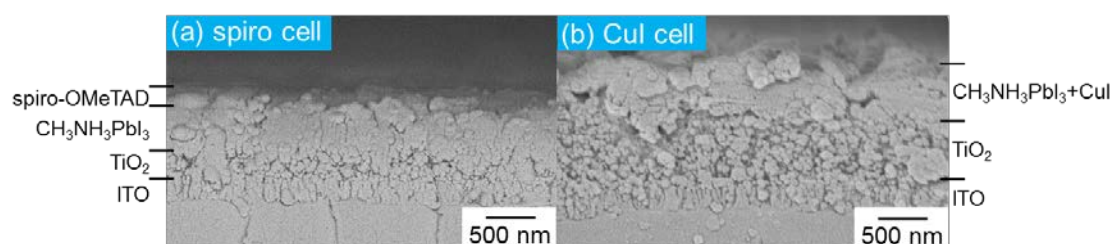Fig. 2. (Color online)

Fig. 3.

Fig. 4. (Color online)

Fig. 5.

Fig. 6. (Color online)